

Ligand effects in carbon-*K*-shell photoionizationS. Fonseca dos Santos,¹ N. Douguet,¹ A. E. Orel,¹ and T. N. Rescigno²¹*Department of Chemical Engineering and Materials Science, University of California, Davis, California 95616, USA*²*Lawrence Berkeley National Laboratory, Berkeley, California 94720, USA*

(Received 7 November 2014; published 9 February 2015)

We consider the effect of substituting atomic ligands X with different electronic properties in the carbon- K -shell photoionization of the linear $XCCX$ molecules. We study the cases of lithium, hydrogen, and fluorine as ligands bonded to the carbon atoms. The molecular frame photoelectron angular distributions are computed using the variational complex Kohn technique. The electronic properties of the ligands have direct observable effects on the angular distribution of the emitted carbon core-hole photoelectron. These effects have already been observed experimentally using the cold target recoil ion momentum spectroscopy technique. We propose a simple classical explanation based on the intramolecular electrostatic potential to qualitatively explain the preferred directions of electron emission.

DOI: [10.1103/PhysRevA.91.023408](https://doi.org/10.1103/PhysRevA.91.023408)

PACS number(s): 33.80.Eh, 98.38.Dq, 95.30.Ft

I. INTRODUCTION

The development of techniques for imaging molecular structure, particularly those techniques which have the potential to be taken into the time domain, are of high current interest in the chemical physics community. Ultrafast electron diffraction [1], femtosecond x-ray diffraction [2], and, most recently, photoelectron diffraction [3] have that potential. In photoelectron diffraction [4], an electron wave is launched by photoabsorption at an inner shell. The outgoing photoelectron wave is then diffracted by the aggregate potential of the molecule. The angular distribution of these electrons, when measured in the body-fixed frame of the molecule [molecular frame photoelectron angular distributions (MFPADs)], is very sensitive to molecular structure. This fact was demonstrated in 2012 in a combined theoretical and experimental study on methane [3,5] which showed that the MFPAD for carbon core-electron photoejection, averaged over all photon polarizations, gives a three-dimensional image of the molecule, with the outgoing electron effectively focused along the bond directions. To measure the angular distributions in the body frame, the orientation of the molecule at the instant of photoionization must either be established through laser alignment [6,7] or, in the case of fragmentation following prompt Auger decay, reconstructed with momentum imaging techniques such as COLTRIMS (COLd target recoil ion momentum spectroscopy) [8,9]. If the time scale of the fragmentation is short compared with the rotational period of the molecule, i.e., if the axial-recoil approximation is fulfilled, then molecular orientation at the time of the photoionization event can be deduced from the ionic product momenta [10].

Although accurate theoretical calculations have proven to be capable of faithfully reproducing the observed angular distributions, the fact is that the underlying mechanisms responsible for the observed imaging remains something of a mystery. Before photoelectron diffraction can be developed into a practical tool for probing molecular and electronic dynamics in ultrafast experiments, it is important to develop an understanding of the factors that determine the shapes of MFPADs and their sensitivity to a molecule's structure and electronic state. For example, the imaging effect found in the core-level MFPADs of simple hydrides that contain a

single heavy atom does not necessarily carry over to more complicated targets. Indeed, the CF_4 molecule provides a striking counterexample [11]. If one represents the tetrahedral CF_4 inside a cube, with the fluorine atoms located on different corners, then the MFPAD, averaged over light polarization directions, shows maxima for photoelectron directions pointing towards the center of each side of the cube. Thus, not only does the MFPAD not image the bonds for this molecule, but the preferred directions of photoelectron emission seem to be avoiding the bonds.

Our purpose here is to investigate this phenomenon in more detail with a view toward gaining some insight into the factors that control the shapes of core-level MFPADs for low photoelectron energies. To that end, we study K -shell photoionization in a series of linear $XCCX$ neutral molecules, with ligands X of different electronegativities. The cases of $X = Li, H,$ and F , are studied and were chosen for their wide range of electro-negativity, from as low as 0.98 (Li), with an intermediate value of 2.20 (H), to a value as high as 3.98 (F). The bonds between the carbon and each ligand present various properties, from quasi-ionic bonds with opposite charge distributions in the cases of lithium and fluorine chemical bonds to a regular valence bond in the case of hydrogen. We show that the difference in the electronic charge density for the $LiCCLi, HCCH,$ and $FCCF$ molecules qualitatively explains the shape of the various MFPADs. We compute the intramolecular electrostatic potential for each molecule and study the electrostatic field and equipotential lines. From the principal aspect of the electrostatic potential, we can give a simple qualitative explanation for the preferred direction of photoelectron emission at energies above ~ 1 eV.

In the next section, we briefly review the theoretical approach used to compute fixed and averaged light polarization MFPADs. The results for $LiCCLi, HCCH,$ and $FCCF$ molecules are given in Sec. IV and discussed in Sec. V. Finally, Sec. VI is devoted to our conclusions.

II. THEORETICAL APPROACH

In this study, the electron-molecular ion scattering is described via the complex Kohn variational method. Since the implementation of the Kohn method in calculations

of photoionization cross sections and photoelectron angular distributions has already been presented in several studies [12–15], we give in the following only the formulas used to compute the MFPADs.

The photoionization cross section is determined from the following matrix elements expressed in terms of body-frame amplitudes:

$$I_{\Gamma_o l_o m_o}^\mu \equiv \langle \Psi_o | \mu | \Psi_{\Gamma_o l_o m_o}^- \rangle \\ = \sum_{i=1}^N \int \Psi_o(r_1, r_N) r_i^\mu \Psi_{\Gamma_o l_o m_o}^-(r_1, r_N) d^3 r_1 \dots d^3 r_N, \quad (1)$$

where r^μ is the dipole operator defined in the length form, Ψ_o is the initial electronic wave function of the neutral molecule, and $\Psi_{\Gamma_o l_o m_o}^-$ is the final-state wave function representing a photoelectron emitted with angular momentum quantum numbers l_o and m_o in the field of a residual molecular ion denoted by Γ_o (see Ref. [16] for details). In our case, Γ_o will either be the σ_u^{-1} or σ_g^{-1} delocalized carbon core-hole state.

The cross-section differential in the angles of photoejection $\Omega_{\hat{k}_o}$ and photon polarization Ω_ϵ relative to the fixed body frame of the molecule is given by

$$\frac{d^2 \sigma^{\Gamma_o}}{d\Omega_{\hat{k}_o} d\Omega_\epsilon} = \frac{8\pi\omega}{3c} |I_{\hat{k}_o, \epsilon}^{\Gamma_o}|^2, \quad (2)$$

where ω is the photon frequency, c is the speed of light, k_o is the momentum of the ejected electron associated with a particular ion channel Γ_o , and $I_{\hat{k}_o, \epsilon}^{\Gamma_o}$ is given by

$$I_{\hat{k}_o, \epsilon}^{\Gamma_o} = \sqrt{\frac{4\pi}{3}} \sum_{l_o m_o \mu} i^{l_o} e^{-i\delta_{l_o}} I_{\Gamma_o l_o m_o}^\mu Y_{1\mu}^*(\hat{\epsilon}) Y_{l_o m_o}^*(\hat{k}_{\Gamma_o}), \quad (3)$$

where δ_{l_o} is the Coulomb phase shift. The angular distribution averaged over all light polarization directions is then simply given as

$$\int \frac{d^2 \sigma^{\Gamma_o}}{d\Omega_{\hat{k}_o} d\Omega_\epsilon} d\Omega_\epsilon = \frac{32\pi^2 \omega}{9c} \sum_{\mu} \left| \sum_{l_o m_o} I_{\Gamma_o l_o m_o}^\mu Y_{l_o m_o}(\hat{k}_{\Gamma_o}) \right|^2. \quad (4)$$

III. COMPUTATIONAL DETAILS

The calculations were performed for a fixed molecular geometry in a two-state coupled-channel approximation using single-configuration wave functions for the $1\sigma_g^{-1}$ and $1\sigma_u^{-1}$ carbon $1s$ core-hole states constructed with neutral self-consistent field molecular orbitals. We used an f -truncated cc-pvtz basis set in order to minimize computational costs. This choice was justified by the results of convergence tests showing that the inclusion of f functions had no net effect on the calculated ionization potential (IP), the energy splitting between the g/u states, and the shape of the computed differential cross sections. In the scattering calculations, the basis set was augmented with diffuse s , p , and d functions for each atom. We also computed MFPADs from two-state calculations using natural orbitals for the molecular target and found only negligible differences with the MFPADs calculated with Hartree-Fock orbitals. We must emphasize that, although the calculated results were found to be insensitive to the details of molecular orbital construction, they are quite sensitive to

the proper coupling of the two core-hole states. Indeed, rather different results are obtained if we ignore electronic channel coupling and compute the MFPADs in an uncoupled (static-exchange) scheme. We have found it essential both here and in core-hole studies on other molecules containing symmetry-equivalent atoms to take explicit account of the coupling between quasidegenerate core-hole states in constructing the final continuum wave functions.

The computed frozen-core (Koopmans') carbon- K -shell ($1\sigma_u^{-1}$) binding energies were found to be 308.92, 305.82, and 301.66 eV for FCCF, HCCH, and LiCCLi, respectively. These energies are ~ 15 eV larger than the experimental ionization energies since they do not account for the orbital relaxation that accompanies ionization. The energy splitting between the σ_u^{-1} and σ_g^{-1} states is approximately 110 meV in HCCH, in agreement with Ref. [17]. The splittings between the σ states in FCCF and LiCCLi were found to be 111 and 78 meV, respectively. Since the small energy splittings between the quasidegenerate g/u states is typically not resolved in most experiments, the MFPADs we present, unless otherwise stated, are summed over both core-hole states.

IV. RESULTS OF CARBON- K -SHELL PHOTOIONIZATION

The carbon- K -shell MFPADs for the HCCH, FCCF, and LiCCLi molecules are presented in Fig. 1 for light polarization along the molecular axis, at five different photoelectron energies. Since we are interested only in the qualitative effects of the substitution of the ligands, the MFPADs were rescaled in the figure in order to present roughly the same magnitude. The molecules are vertically aligned and the different shape of the MFPADs in FCCF, when compared to those for HCCH and LiCCLi, can easily be seen. In the case of FCCF, the relative magnitude for emissions along the plane perpendicular to the molecule becomes larger than the emissions along the axis of the molecule as the photoelectron energy increases. This clearly indicates a propensity for the photoelectron to avoid the fluorine atoms as it exits the molecule. On the other hand, the MFPADs for both HCCH and LiCCLi images the molecular bonds for all energies considered. The imaging effect seems to occur to a greater extent for LiCCLi, and is more pronounced at higher energies.

Figure 2 shows the MFPADs at the same five energies but with the light polarization averaged over all angles [see Eq. (4)]. Compared to the cases of polarization fixed along the molecular axis, the imaging effect is seen to be less pronounced for HCCH at higher energies and for LiCCLi at lower energies. However, the effect of fluorine as a ligand is still present showing increasing perpendicular emission, which remains absent in HCCH and LiCCLi.

Plesiat *et al.* [18] have recently reported C ($1s^{-1}$) MFPADs for HCCH obtained from static-exchange density functional calculations. Their results differ markedly from ours. To understand the discrepancy, we repeated our calculations at 3-eV photoelectron energy. The results are shown in Fig. 3. While our coupled two-state results differed little in shape from what we found at 2 and 4 eV, they are at complete odds with the 3-eV results of Plesiat *et al.* However, when we repeated the calculations using uncoupled static-exchange wave functions for the core-hole states, we found results similar to theirs.

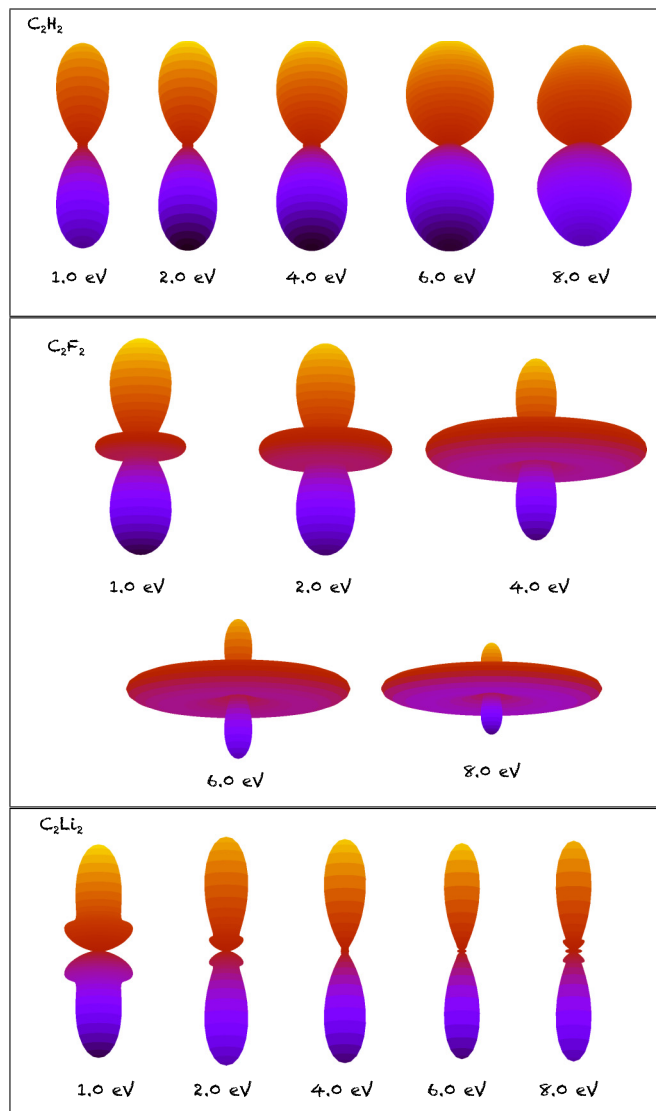


FIG. 1. (Color online) Carbon $1s^{-1}$ MFPADs with light polarization along the molecule axis for HCCH, FCCF, and LiCCLi at 1.0, 2.0, 4.0, 6.0, and 8.0 eV. The molecular axes are oriented vertically. The MFPADs were rescaled to the same maximum magnitude.

We emphasize again that at low photoelectron energies, it is essential to include coupling between quasidegenerate channels.

V. DISCUSSION

The detailed features of the MFPADs can only be explained in terms of quantum effects and wave functions, especially at very low photoelectron energy. However, one can invoke a simple argument based on the electronic charge distribution in each molecule to explain the general trends found in the distributions. Because an atom with small electronegativity, such as lithium, acquires a net positive charge through bonding with the carbon atom, the emitted carbon core-hole electron is more attracted towards the lithium atom. Therefore, the molecular axis becomes the privileged direction of photoelectron emission. On the other hand, when an atom with

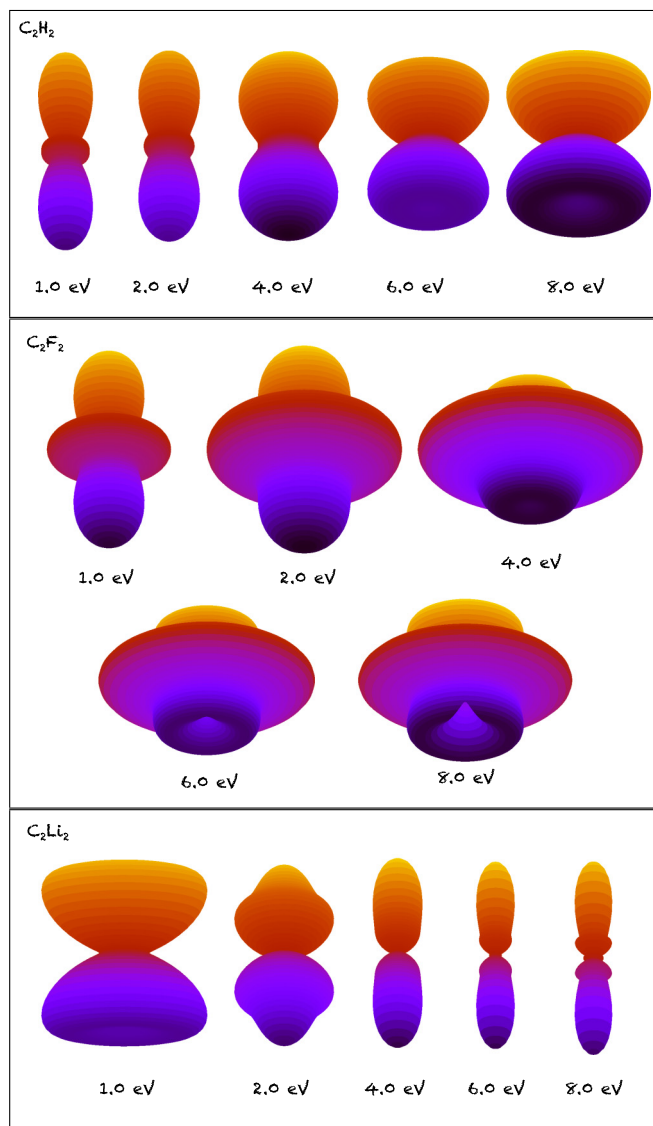


FIG. 2. (Color online) As in Fig. 1, with averaged light polarization.

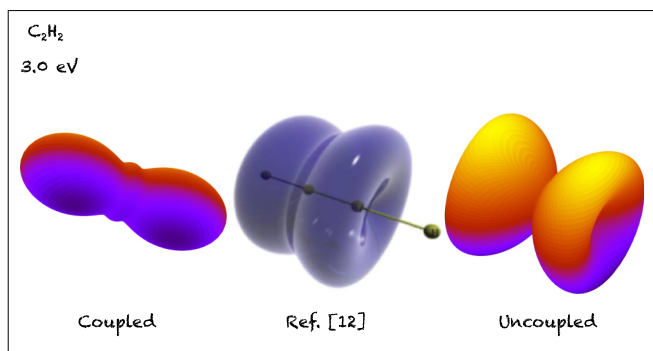


FIG. 3. (Color online) Carbon $1s^{-1}$ MFPADs with averaged light polarization for HCCH at 3.0-eV photoelectron energy. Coupled two-channel results are compared with uncoupled static-exchange results and the results of Ref. [18].

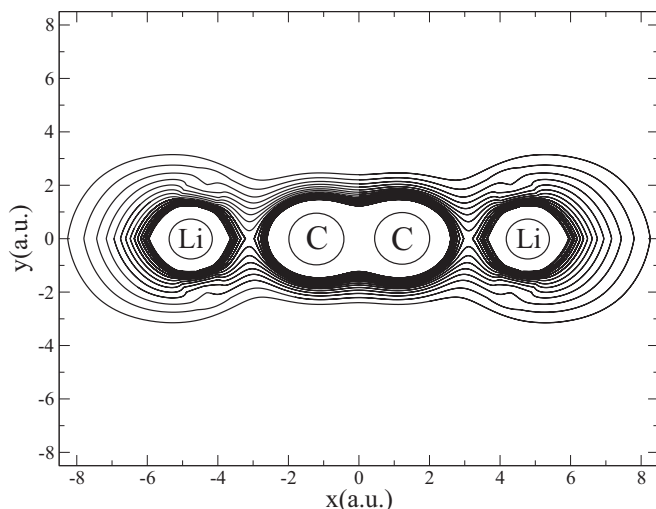


FIG. 4. Electrostatic intramolecular equipotential lines for the $1\sigma_u^{-1}$ carbon core-hole electronic state of $C_2Li_2^+$. The equipotential lines are plotted from -30 to -6 eV, with a constant energy step size of 1 eV.

high electronegativity, such as fluorine, binds to the carbon atom, it acquires a net negative charge. In this case, the photoelectron emitted from the tightly bound carbon- K -shell molecular orbital tends to avoid the region of high electron density that resides close to the fluorine atom. Hence, in the classical picture, the photoelectron is deflected by the fluorine electronic cloud, such that it scatters preferentially away from the molecular axis.

This qualitative argument can be made somewhat more concrete by a more quantitative analysis. If the shape of the MFPADs could be in part explained by the electron density inside the molecule, then it should also be equally reflected by the static potential seen by the photoelectron:

$$V(\vec{r}) = \int \frac{\rho(\vec{r}')}{|\vec{r} - \vec{r}'|} d^3\vec{r}' - \sum_a \frac{Z_a}{|\vec{r} - \vec{R}_a|}, \quad (5)$$

where $\rho(\vec{r}')$ is the electronic charge density of a molecular ion core-hole state, calculated with the Hartree-Fock molecular orbitals employed in the complex Kohn calculations, and the second term on the right-hand side of Eq. (5) is the attractive potential due to the nuclei located at position \vec{R}_a and with atomic number Z_a . One expects $V(\vec{r})$ to be drastically different for the case studies of the $LiCCLi^+$, $HCCH^+$, and $FCCF^+$ molecular ions.

A plot of the equipotential surfaces offers a convenient way to visualize the electrostatic potential. Since the molecules under study have cylindrical symmetry, we can simply draw the equipotential lines corresponding to the intersection of the equipotential surfaces with any given plane containing the molecular axis. The calculated equipotential lines are shown for $LiCCLi^+$ ($1\sigma_g^{-1}$), $HCCH^+$ ($1\sigma_g^{-1}$), and $FCCF^+$ ($2\sigma_g^{-1}$) in Figs. 4, 5, and 6, respectively. The x and y directions are plotted on the same scale to avoid unphysical distortions of the equipotential lines. Note that $V(\vec{r})$ has little dependence on the actual g/u symmetry of the tightly bound molecular orbitals because there is negligible overlap between the carbon

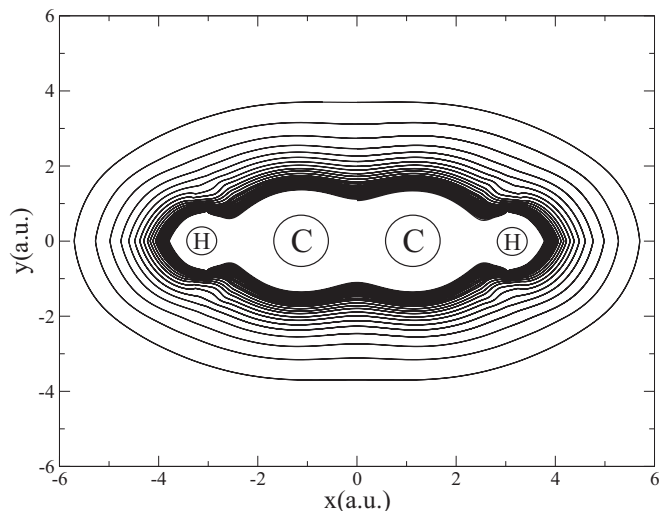


FIG. 5. As in Fig. 4, for the $1\sigma_u^{-1}$ carbon core-hole electronic state of $C_2H_2^+$.

$1s$ orbitals. For this reason, we only show a single-symmetry case of electrostatic potential for each molecule.

In Figs. 4–6, the equipotential lines are drawn from -30 eV (inner region) to -6 eV (outer region), with a constant energy step size of 1 eV. A constant step size was chosen in order to easily visualize the region of high density of lines, where the electrostatic field is the strongest. From the figures, it is clear that the electrostatic potentials are different for the three core-hole photoions and the equipotential lines in $HCCH^+$ represent the intermediate situation between the two extreme cases of $LiCCLi^+$ and $FCCF^+$. Note, in particular, the density and shape of the equipotential lines just around the molecular cores. In $LiCCLi^+$, the density of equipotential lines is the largest in directions orthogonal to the molecular axis, as if the lines were squeezed around the axis. On the other hand, at the edges of the molecule, near the lithium atoms, the density of lines, and thus the field, is the lowest. This means that the

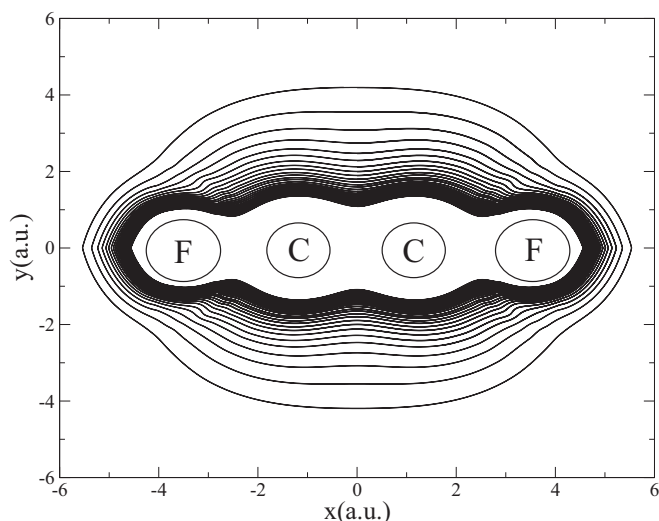


FIG. 6. As in Fig. 4, for the $2\sigma_g^{-1}$ carbon core-hole electronic state of $C_2F_2^+$.

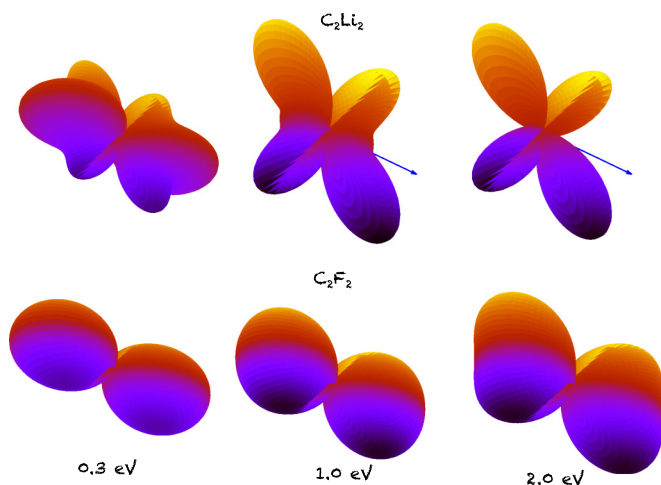


FIG. 7. (Color online) Carbon $1\sigma_g^{-1}$ MFPADs with light polarization along the x axis (blue arrow), perpendicular to the molecular axis, for LiCCLi (top) and FCCF (bottom) at 0.3, 1.0, and 2.0 eV. The molecular axes are oriented vertically and the MFPADs are rescaled.

restoring intramolecular electrostatic forces experienced by the electron are much stronger in directions orthogonal to the axis than parallel to it. Therefore, an oscillating field applied onto the molecule will drive the electron most efficiently along the molecular axis. This means that the potential that the electron should overcome to escape the molecule is much steeper in the direction orthogonal to the molecular axis. The opposite situation arises in the case of FCCF⁺ for which the density of lines is the largest at the edge of the molecular axis, near the fluorine atoms. In this situation, it is clear that an oscillating field orthogonal to the molecular axis would efficiently drive the electron there in contrast to the case of LiCCLi⁺. The equipotential lines in HCCH⁺ clearly represent an intermediate case. Although it remains more efficient for the photoelectron to reach an outer equipotential line along the molecular axis, at sufficiently large energy, the electron can also escape the attractive electrostatic potential in directions away from the molecular axis. Equipotential lines above -6 eV were not plotted since they are less interesting. The higher-energy lines start to spread rapidly at large distance from the molecule and become simple circles as the Coulomb field of the residual positive unit charge begins to strongly dominate all higher multipole terms.

Finally, we consider in more detail the MFPADs of LiCCLi and FCCF for light polarization perpendicular to the molecular axis. As an example, Fig. 7 shows MFPADs for x -polarized light at three photoelectron energies in the σ_g^{-1} channel in total Π_{u_x} symmetry. The difference in behavior for both molecules is striking. While for FCCF the shape of the MFPADs is

almost constant with energy, for LiCCLi there is a pronounced reshaping above the first energy. We explain this difference in terms of interference of the photoelectron partial waves, as discussed in Ref. [19], combined with the effect of the ligand electronegativity. For lithium, we see that at 0.3 eV, where the effect of the lowest symmetry-allowed partial wave is most pronounced, the main contribution comes from the $l = 1$ (p_x) partial wave. However, perpendicular emission in LiCCLi is not the preferred path for the photoelectron, as discussed previously. Therefore, as soon as the contribution from the higher symmetry-allowed partial waves starts to increase, the shape of the MFPAD markedly changes. Indeed, it starts to show increasing features of the $l = 3$ partial wave, with its perpendicular lobes absent due to destructive interference with the $l = 1$ partial wave. Thus, the electron avoids scattering in the unfavorable perpendicular direction. The same effect is not present for FCCF. Because it is efficient for the electron to be emitted perpendicularly to the axis of the molecule, the p_x wave dominates for all the selected energies and the shape of the MFPADs remains nearly constant.

VI. CONCLUSION

We have shown that the carbon- K -shell MFPADs of the three molecular systems under consideration exhibit markedly different characteristics. In LiCCLi, the photoelectron is preferentially emitted along the molecular axis at all energies considered. In HCCH, the molecular axis is also the preferred direction for emission; however, the angular spreading for photoelectron emission around this axis is significantly larger and increases with the photoelectron energy. In contrast, the carbon core-hole MFPADs for FCCF show significant propensity for photoemission in the angular region orthogonal to the molecular axis at the energies considered. These results seem to corroborate previous theoretical and experimental findings on carbon- K -shell photoionization of CH₄ [3] and CF₄ [11]. The electron is emitted mostly along the C-H bonds in the former case, whereas it is emitted in directions avoiding the C-F bonds in the latter case.

ACKNOWLEDGMENTS

Work at University of California Lawrence Berkeley National Laboratory was performed under the auspices of the US Department of Energy under Contract No. DE-AC02-05CH11231 and was supported by the US DOE Office of Basic Energy Sciences, Division of Chemical Sciences. A.E.O. acknowledges support by the National Science Foundation, with some of this material being based on work done while serving at the NSF.

- [1] A. H. Zewail, *Science* **328**, 187 (2010).
 [2] H. N. Chapman *et al.*, *Nature (London)* **470**, 187 (2011).
 [3] J. B. Williams *et al.*, *Phys. Rev. Lett.* **108**, 233002 (2012).
 [4] A. Landers *et al.*, *Phys. Rev. Lett.* **87**, 013002 (2001).
 [5] J. B. Williams *et al.*, *J. Phys. B: At., Mol. Opt. Phys.* **45**, 194003 (2012).

- [6] J. J. Larsen, K. Hald, N. Bjerre, H. Stapelfeldt, and T. Seideman, *Phys. Rev. Lett.* **85**, 2470 (2000).
 [7] J. L. Hansen, L. Holmegaard, L. Kalthøj, S. L. Kragh, H. Stapelfeldt, F. Filsinger, G. Meijer, J. Küpper, D. Dimitrovski, M. Abu-samha *et al.*, *Phys. Rev. A* **83**, 023406 (2011).

- [8] J. Ullrich, R. Moshhammer, A. Dorn, R. Dörner, L. P. H. Schmidt, and H. Schmidt-Böcking, *Phys. Rep.* **330**, 95 (2000).
- [9] J. Ullrich, R. Moshhammer, A. Dorn, R. Dörner, L. Ph. H. Schmidt, and H. Schmidt-Böcking, *Rep. Prog. Phys.* **66**, 1463 (2003).
- [10] T. Osipov, M. Stener, A. Belkacem, M. Schöffler, Th. Weber, L. Schmidt, A. Landers, M. H. Prior, R. Dörner, and C. L. Cocke, *Phys. Rev. A* **81**, 033429 (2010).
- [11] C. Trevisan, J. Williams, A. Menssen, T. Weber, T. Rescigno, C. W. McCurdy, and A. Landers, *Bull. Am. Phys. Soc.* **59**, K1.0013 (2014).
- [12] C. S. Trevisan, C. W. McCurdy, and T. N. Rescigno, *J. Phys. B: At., Mol. Opt. Phys.* **45**, 194002 (2012).
- [13] T. N. Rescigno, N. Douguet, and A. E. Orel, *J. Phys. B: At., Mol. Opt. Phys.* **45**, 194001 (2012).
- [14] A. E. Orel, T. N. Rescigno, and B. H. Lengsfeld, *Phys. Rev. A* **44**, 4328 (1991).
- [15] N. Douguet, T. N. Rescigno, and A. E. Orel, *Phys. Rev. A* **88**, 013412 (2013).
- [16] T. N. Rescigno, B. H. Lengsfeld III, and A. E. Orel, *J. Chem. Phys.* **99**, 5097 (1993).
- [17] H. Bash and L. C. Snyder, *Chem. Phys. Lett.* **3**, 333 (1969).
- [18] E. Plesiat, P. Decleva, and F. Martin, *Phys. Rev. A* **88**, 063409 (2013).
- [19] S. Miyabe, C. W. McCurdy, A. E. Orel, and T. N. Rescigno, *Phys. Rev. A* **79**, 053401 (2009).